



Automatic pectoral muscle segmentation on mediolateral oblique view mammograms

Kwok, S.M.; Chandrasekhar, R.; Attikiouzel, Y.; et.al.

<https://researchportal.murdoch.edu.au/esploro/outputs/journalArticle/Automatic-pectoral-muscle-segmentation-on-mediolateral/991005540304107891/filesAndLinks?index=0>

Kwok, S. M., Chandrasekhar, R., Attikiouzel, Y., & Rickard, M. T. (2004). Automatic pectoral muscle segmentation on mediolateral oblique view mammograms. *IEEE Transactions on Medical Imaging*, 23(9), 1129–1140. <https://doi.org/10.1109/TMI.2004.830529>

Document Version: Published (Version of Record)

Published Version: <https://doi.org/10.1109/TMI.2004.830529>



MURDOCH RESEARCH REPOSITORY

<http://dx.doi.org/10.1109/TMI.2004.830529>

**Kwok, S.M., Chandrasekhar, R., Attikiouzel, Y. and Rickard, M.T.
(2004) Automatic pectoral muscle segmentation on
mediolateral oblique view mammograms. IEEE Transactions on
Medical Imaging, 23 (9). pp. 1129-1140.**

<http://researchrepository.murdoch.edu.au/20165/>

Copyright © 2004 IEEE

Personal use of this material is permitted. However, permission to reprint/republish this material for advertising or promotional purposes or for creating new collective works for resale or redistribution to servers or lists, or to reuse any copyrighted component of this work in other works must be obtained from the IEEE.

Automatic Pectoral Muscle Segmentation on Mediolateral Oblique View Mammograms

Sze Man Kwok, Ramachandran Chandrasekhar*, *Member, IEEE*, Yianni Attikiouzel, *Fellow, IEEE*, and Mary T. Rickard

Abstract—Mammograms are X-ray images of the breast which are used to detect breast cancer. When mammograms are analyzed by computer, the pectoral muscle should preferably be excluded from processing intended for the breast tissue. For this and other reasons, it is important to identify and segment out the pectoral muscle. In this paper, a new, adaptive algorithm is proposed to automatically extract the pectoral muscle on digitized mammograms; it uses knowledge about the position and shape of the pectoral muscle on mediolateral oblique views. The pectoral edge is first estimated by a straight line which is validated for correctness of location and orientation. This estimate is then refined using iterative “cliff detection” to delineate the pectoral margin more accurately. Finally, an enclosed region, representing the pectoral muscle, is generated as a segmentation mask. The algorithm was found to be robust to the large variations in appearance of pectoral edges, to dense overlapping glandular tissue, and to artifacts like sticky tape. The algorithm has been applied to the entire Mammographic Image Analysis Society (MIAS) database of 322 images. The segmentation results were evaluated by two expert mammographic radiologists, who rated 83.9% of the curve segmentations to be adequate or better.

Index Terms—Automatic segmentation, cliff detection, mammogram, pectoral muscle, straight line estimation.

I. INTRODUCTION

X-RAY mammography is the most widely used method to screen asymptomatic women for early detection of breast cancer. The large number of mammograms generated by population screening must be interpreted and diagnosed by relatively few radiologists. It is considered that the use of computerized mammographic analysis will make a vital contribution to easing the increasing workload and assisting in the detection of breast

cancer. We contend that before the digitized mammogram is analyzed by computer, it must be segmented into its representative anatomical regions. Three anatomical *landmarks* have to be first extracted automatically: they are the breast border [1], the nipple [2] and the pectoral muscle [3]. In this paper, we propose a method for automatically segmenting the pectoral muscle on mediolateral oblique (MLO) view mammograms.

When the MLO view is properly imaged, the pectoral muscle should always appear as a high-intensity, triangular region across the upper posterior margin of the image. The cranio-caudal (CC) view is not considered in this paper because the pectoral muscle is only seen in about 30%–40% of CC images [4]. Several factors complicate the segmentation of the pectoral muscle. Depending on anatomy and patient positioning during image acquisition, the pectoral muscle could occupy as much as half of the breast region, or as little as a few percent of it. The curvature of the muscle edge is usually convex, but it can also be concave, or a mixture of both. Although the pectoral muscle boundary is perceived to be visually continuous by humans, there are large variations in edge strength and texture. In many cases the upper part of the boundary is a sharp intensity edge while the lower part is more likely to be a texture edge, due to the fact that it is overlapped by fibro-glandular tissue. In addition, the muscle edge may be obscured by artifacts on the digitized mammogram, such as sticky tapes. Because of all these factors, automatic segmentation of the pectoral muscle by computer is a demanding task.

Automatic pectoral muscle segmentation is useful in many areas of mammographic analysis. The work of Gupta and Undrill [5] indicates that mammographic parenchyma and the pectoral region may have similar texture characteristics, causing a high number of false positives when detecting suspicious masses. In other words, the pectoral muscle could interfere with automated detection of cancers. Also the area overlying the pectoral muscle is a common area for cancers to develop and is particularly checked by radiologists to reduce false negatives. It is, therefore, necessary to segment out the pectoral muscle before lesion detection, as stated in [6]. Similarly, exclusion of the pectoral muscle is required for automatic breast tissue density quantification [7], [8]. The pectoral edge is also used as one of the axes in 3-dimensional reconstructions from multiple mammographic views [9], [10]; and it is one of the pivotal landmarks in mammogram-pair registration and comparison [11]. Furthermore, it is recommended by radiologists that, for a high-quality MLO mammogram, the pectoral muscle should be seen to the level of the nipple or below [4], [12], [13]. Some authorities have recommended, in addition, that the pectoral margin should be convex [4], [12]; that the angle made by the margin with the image edge should not be less than 20° [14];

Manuscript received November 30, 2003; revised April 16, 2004. This work was supported in part by The University of Western Australia under UWA Small Grant 12104000, by Australian Research Council (ARC) Large Grant A00000714, and by the Western Australian Government through funding of the Australian Research Centre for Medical Engineering (ARCME) as part of its *Centres of Excellence* programme. The Associate Editor responsible for coordinating the review of this paper and recommending its publication was S. R. Ayilward. Asterisk indicates corresponding author.

S. M. Kwok and Y. Attikiouzel are with the Centre for Intelligent Information Processing Systems, School of Electrical, Electronic and Computer Engineering, The University of Western Australia, Crawley, WA 6009, Australia. (e-mail: kwok-sm@ee.uwa.edu.au; yianni@ee.uwa.edu.au).

*R. Chandrasekhar is with the Centre for Intelligent Information Processing Systems, School of Electrical, Electronic and Computer Engineering, The University of Western Australia, Crawley, WA 6009, Australia. (e-mail: chandra@ee.uwa.edu.au).

M. T. Rickard is with BreastScreen NSW Corporate, Westmead Hospital, Westmead NSW 2145, Australia (e-mail: maryr@bsnsw.org.au).

Digital Object Identifier 10.1109/TMI.2004.830529

and that the quality of the pectoral margin may be assessed on a numerical scale [13]. Hence extracting the pectoral edge, as both straight line and curve, is particularly important in automatic evaluation of mammographic adequacy [15].

A. Literature Review

The Hough transform, used by Karssemeijer [7] to detect the pectoral edge, is a popular technique. This method assumes that the pectoral edge is approximately a straight line oriented in a certain direction. To ensure that the correct peak is selected in the Hough space, gradient magnitude and orientation, length of projected line, and corresponding pectoral area were taken into account. Because of this careful selection scheme, the results were claimed to be very robust and reliable [7]. Other recent studies based on the Hough transform include: Ferrari *et al.* [16] who segmented mammograms into skin-air boundary, fibro-glandular tissue, and pectoral muscle; Yam *et al.* [9] who refined the Hough transform linear approximation into a curved pectoral boundary using a dynamic programming method; and Georgsson [10] who extracted the pectoral muscle by region growing, but later found the Hough transform to be more reliable.

There are several other approaches to segment the pectoral muscle. Suckling *et al.* [17] segmented mammograms into four major components: background, pectoral muscle, fibro-glandular region and adipose region, using multiple, linked self-organizing neural networks. Aylward *et al.* [18] used a gradient magnitude ridge traversal algorithm at a small scale to extract multiple initial points and then resolved the resulting multiple edge definitions via a voting scheme. Their method parallels that of Karssemeijer [7]. Saha *et al.* [8], [19] reported a semi-automatic method that requires input from an operator to locate the pectoral muscle; delineation is then performed automatically. Chandrasekhar and Attikouzel proposed two techniques to enhance the pectoral muscle region on mammograms: the extended Russ operator [20], and tunable parametric edge detection [21], although final segmentation on the enhanced images had not been carried out.

In summary, almost all of the previous work approximates the pectoral edge as a straight line and then refines that straight line into a more accurate curved boundary, if needed. The accuracy of straight line approximation is usually good. With the Hough transform, the pectoral muscle was segmented in 92.8% of the mammograms tested in [7]; and the pectoral muscle was *accurately* detected in 87.9% of the images within a difference of 1–3 mm in [16]. However the reliability of curve refinement has not been specifically tested and reported in the literature. In our approach, presented in this paper, this two-step process is taken as the basis, and extended by iteration to confer robustness. But the algorithms used by us to derive the straight line and the curve are fundamentally different from existing methods. Several techniques are also introduced to overcome failure due to poor breast positioning and artifacts, and to validate the straight line approximation before it is refined to a curve. The final segmentation results have been thoroughly assessed by two mammographic experts. An early version of this work was described in [3].

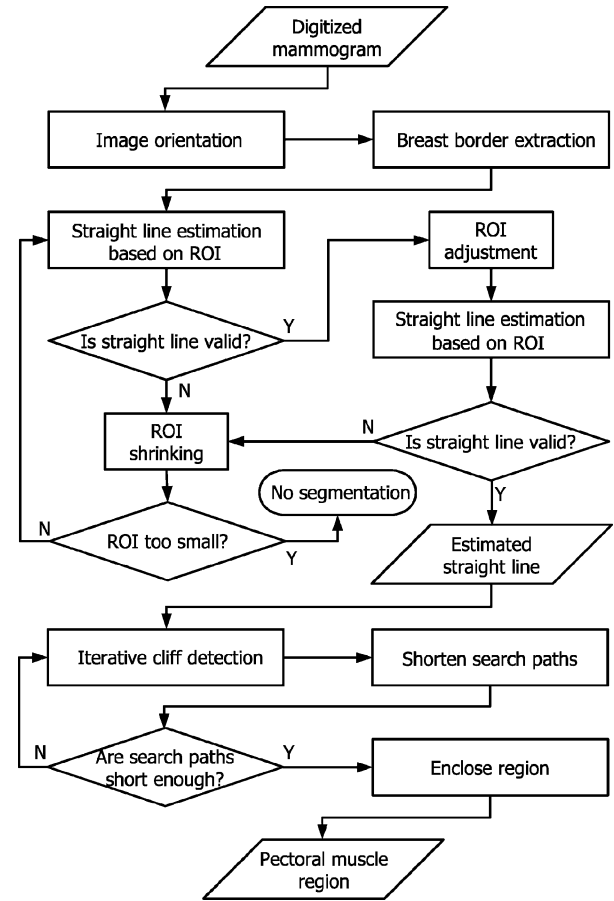


Fig. 1. Flowchart for automatic pectoral muscle segmentation on MLO mammograms. The image orientation and breast border extraction are preprocessing steps that are not part of this algorithm.

II. OVERALL ALGORITHM

From the observations made in Section I regarding the appearance of the pectoral region, we frame the following four hypotheses that form the foundation for the algorithm:

- 1) On mediolateral oblique mammograms, the pectoral muscle is a roughly *triangular region* occupying a corner of the mammogram.
- 2) The pectoral muscle is defined as a region of *higher* intensity than the surrounding tissue.
- 3) The pectoral margin is characterized by a fairly sharp change in intensity, i.e., it is an *intensity edge*.
- 4) The intensity edge can be located by fitting step functions to a sequence of the intensity profiles which lie perpendicular to the pectoral boundary. The step-transition point represents the position of the edge.

Because the pectoral margin may be and is usually curved, it is first estimated as a straight line, which is later refined to a curve. The algorithm, therefore, consists of two main steps: a) straight line estimation; and b) iterative cliff detection. The flowchart of this algorithm is shown in Fig. 1.

There are two preprocessing steps: image orientation and breast border extraction. The image is first oriented in portrait mode to face the same direction for consistency, as shown in Fig. 2. In the MIAS database [22], the image dimensions and left/right labels are already given, so only image rotation and mirroring are required. The breast border is then extracted

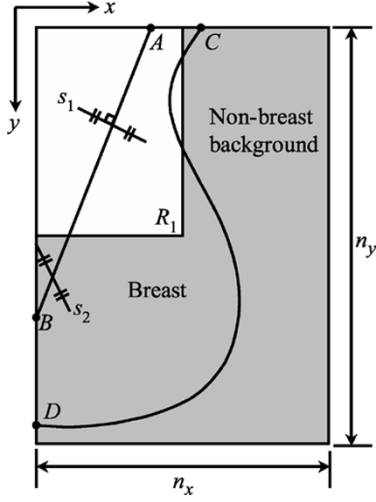


Fig. 2. The mammogram is oriented so that the pectoral muscle is located at the top left corner. The coordinate axes are directed as shown with the origin also at the top left corner. The width and height of the whole image are denoted by n_x and n_y , respectively. R_1 is the initial region of interest, equivalent to one quarter of the image. The straight line AB is an approximation to the pectoral edge. The end-points of the breast border are C and D . s_1 represents a search path perpendicular to AB whereas s_2 represents a rotated search path.

automatically by background modeling and subtraction [1]. The accuracy of the extracted border does not significantly affect the performance of pectoral muscle segmentation, since the breast border is only used for validation and the endpoints of the border are chosen cautiously (as explained in Section IV-B1).

The first part of the segmentation algorithm generates a straight line approximating the pectoral edge. The initial straight line estimation is carried out within a region of interest (ROI). The straight line is then tested for validity. If valid, the ROI is adjusted accordingly, and a second straight line estimation is performed in the new ROI. If the second straight line is also valid, it is used as the input to iterative cliff detection.

If the straight line is found to be not valid at any stage, the ROI is shrunk to a smaller size and the estimation cycle repeated. When the ROI is smaller than a certain size, the algorithm terminates with no segmentation of the pectoral muscle.

The second part of the algorithm is iterative cliff detection in which the straight line is refined to a curve that more accurately depicts the pectoral margin. This is an iterative process whereby the detected curve is fed back to the cliff detection module for increased accuracy. Finally, the “triangle” with the detected pectoral margin as hypotenuse, is closed to give a segmentation mask for the pectoral muscle.

III. ORIENTATION AND NOTATION

In our segmentation algorithm, all digitized mammograms are oriented so that the nipple faces the right, i.e., all the right breast images are mirrored vertically. Therefore, all input images are always upright with the pectoral muscle at the top left corner. The intensity of the image is denoted by $I(x, y)$ in the range $[0, I_{\max}]$. The origin of the coordinate system is at the top left corner of the image, where x is defined to be the horizontal axis and y to be the vertical one (see Fig. 2). The number of pixels of the image in the x and y directions are denoted by n_x and n_y , respectively. Parameters used in the algorithm are given

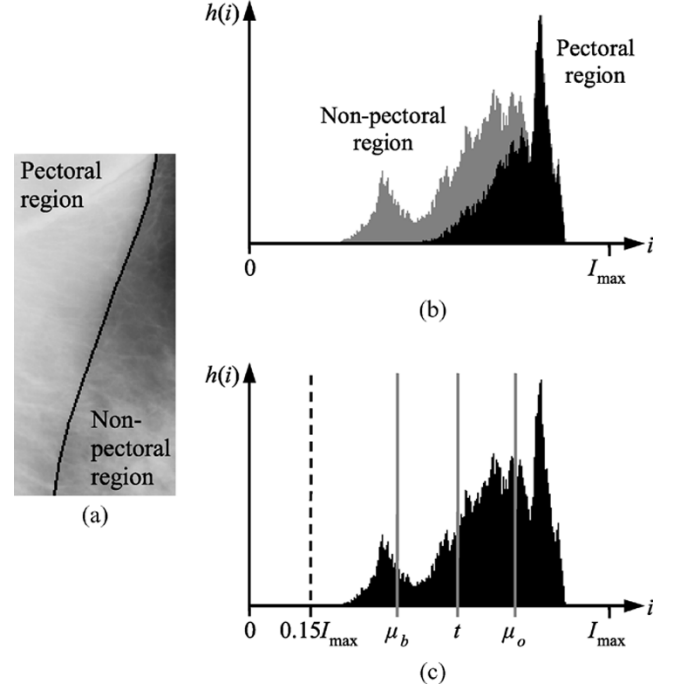


Fig. 3. (a) Pectoral and nonpectoral regions in the initial ROI, R_1 . The spatial overlap of pectoral muscle and glandular tissue can be seen in the lower portion. The region boundary was traced out by hand. (b) Intensity histogram, $h(i)$, of R_1 showing the intensity overlap of the pectoral (black) and nonpectoral (grey) regions corresponding to (a). (c) Iterative threshold selection, where grey-levels below 15% of I_{\max} are excluded (left of dotted line); μ_b and μ_o are the mean values of the background and object grey-levels, respectively; and t is the final threshold.

in millimeters; they may be converted to pixels if divided by the image resolution in mm/pixel.

IV. STRAIGHT LINE ESTIMATION AND VALIDATION

Straight line estimation is used to approximate the pectoral muscle with a straight line. This algorithm is based on iterative threshold selection and straight line fitting with a gradient test. The result is then validated by a simple criterion, independently of the straight line fit.

A. Straight Line Estimation

1) *Defining the Region of Interest (ROI)*: Since the pectoral muscle is located at the top left corner of the image, the *top left quarter* of the image is taken to be the initial region of interest (ROI), as shown in Fig. 2. It is assumed that the pectoral edge appears in this ROI (partially, if not fully) and that it intersects the top and left image edges. The first straight line estimation of pectoral edge is performed in this ROI, which is represented by R_1 where

$$R_1 = \left\{ (x, y) : 0 \leq x < \frac{n_x}{2} \text{ and } 0 \leq y < \frac{n_y}{2} \right\}. \quad (1)$$

Fig. 4(a) shows the initial ROI of mammogram mdb227lm taken from the MIAS database [22].

2) *Iterative Threshold Selection*: After setting the initial ROI, the pectoral muscle (pectoral region) should be separated from other tissues (nonpectoral region) as it has been done *manually* in Fig. 3(a). However, determining a global threshold

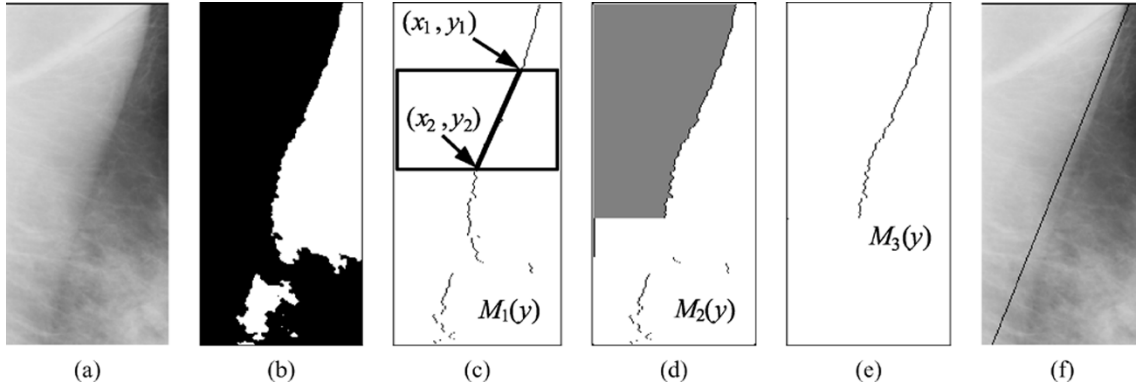


Fig. 4. Illustration of straight line estimation. (a) Initial ROI of MIAS image mdb227lm. (b) Median filtered binary image produced by iterative threshold selection. (c) $M_1(y)$, obtained by tracing the border of black region. Its gradient is computed in the sliding window. (d) $M_2(y)$, result of removing positive gradient segments, with the largest area under the curve shaded. (e) $M_3(y)$, selected for straight line fitting. (f) Straight line approximation to the pectoral edge.

automatically is not straightforward. In many MLO mammograms, the lower portion of the pectoral muscle is spatially superimposed on some glandular tissue known as the “tail of Spence” [4]. Also, the image intensity of the glandular tissue can be very near or identical to that of the pectoral muscle, causing intensity overlap of the pectoral and nonpectoral regions in the histogram [see Fig. 3(b)].

Due to both *spatial and intensity overlaps* of the two regions, it is not always possible to find a single threshold that completely separates the pectoral muscle from other tissues. However, *iterative threshold selection* can be used to optimize the conversion of the grey-scale image to a binary image in the sense that the image average luminance is preserved; this is explained and mathematically proven in [23]. This method usually works well even if the histogram is not bi-modal [24, p. 129]. For the images affected by intensity overlap, iterative threshold selection is less likely to over- or under-estimate the threshold when compared with other techniques that place the threshold at the valley between two peaks in the histogram.

The algorithm given below has been slightly modified from that given in [24, pp. 129–130] and assumes that the image has two regions of dominant grey-levels:

- i) All grey-levels below 15% of I_{\max} are removed from the histogram, $h(i)$, of the region R_1 . It is assumed that the non-breast background and the majority of the breast-edge tissue have been excluded to ensure that the segmentation result is more reliable.
- ii) A threshold t is determined as the mean of all remaining pixel values in R_1

$$t = \frac{\sum_{i \geq 0.15I_{\max}} i \cdot h(i)}{\sum_{i \geq 0.15I_{\max}} h(i)}. \quad (2)$$

- iii) The region R_1 is segmented into background and object by thresholding at t .
- iv) The mean values of the background and object grey-levels, denoted by μ_b and μ_o ,

respectively, are calculated by the following equations:

$$\mu_b = \frac{\sum_{0.15I_{\max} \leq i < t} i \cdot h(i)}{\sum_{0.15I_{\max} \leq i < t} h(i)} ; \quad \mu_o = \frac{\sum_{i \geq t} i \cdot h(i)}{\sum_{i \geq t} h(i)}. \quad (3)$$

- v) t is then updated as the mid-point of μ_b and μ_o

$$t = \frac{\mu_o + \mu_b}{2}. \quad (4)$$

- vi) If the new t remains unchanged, it is the final threshold; otherwise steps iii)–vi) are repeated.

3) *Pixel Selection*: After thresholding, the edge of the pectoral muscle has to be traced out on the binary image [Fig. 4(b)] by a *pixel selection* operation. First, impulse noise on the binary image is removed by applying a 5×5 median filter. Then each horizontal line of the binary image is scanned from left to right, and the *first* background pixel on each scan line is selected. The positions of all the selected pixels define the function $M_1(y)$, that roughly represents the pectoral edge.

4) *Gradient Test*: If the selected pixels $M_1(y)$ represent the actual pectoral edge accurately, straight line fitting can be applied to it directly. However, in some cases, the curve $M_1(y)$ deviates toward the right and forms a concave segment, whenever the glandular tissue overlaps the pectoral edge. The deviation from the actual edge may lead to an inaccurate straight line estimation.

A *gradient test* was, therefore, designed to eliminate the concave segments on the function $M_1(y)$. A sliding window of height 20 mm and width equal to the ROI is used in the test. As the window slides from top to bottom, a straight line is fitted to the portion of $M_1(y)$ that lies within the window, and the gradient of the fitted line is computed [see Fig. 4(c)]. The gradient function, $g(y)$, is given by

$$g(y) = \frac{x_2 - x_1}{y_2 - y_1} \quad \text{for} \quad \frac{y_2 - y_1}{2} < y < \frac{n_y}{2} - \frac{y_2 - y_1}{2} \quad (5)$$

where (x_1, y_1) and (x_2, y_2) are the end-points of the fitted line, and $n_y/2$ is the height of R_1 .

Normally, $g(y)$ is *negative* when $M_1(y)$ is a decreasing function which represents the actual pectoral edge. If there is a deviation from the pectoral edge, $g(y)$ becomes *positive*. Hence in order to eliminate the concave deviations, $M_1(y)$ is set to zero whenever $g(y)$ is nonnegative. Consequently the remaining pixels form a new function $M_2(y)$, which may consist of discontinuous segments. Note that $g(y)$ is undefined at both ends of the ROI and $M_1(y)$ would not be set to zero there.

5) *Straight Line Fitting*: Although the concave deviations have been removed, some small, discontinuous segments left in $M_2(y)$ may also affect the accuracy of the straight line estimation. Therefore, only the *continuous segment with the largest area under the curve* [shown shaded in Fig. 4(d)] is used for straight line fitting because it is most likely to be the actual pectoral edge. This segment is represented by a third function $M_3(y)$ in Fig. 4(e). Straight line fitting with least squared error is then applied to $M_3(y)$ and results in the *first* straight line approximation to the pectoral edge, as shown in Fig. 4(f). This line is shown as \overline{AB} in Fig. 2.

B. Straight Line Validation

1) *Validation Criterion*: A simple criterion is used to validate the straight line estimation. Line \overline{AB} must intersect the top and left image edges inside the breast region, but the intersections may not be inside the ROI. To define the breast region, the breast border $(x_{\text{border}}, y_{\text{border}})$ was extracted automatically by polynomial modeling [1]. Since this method is not immune to artifacts from tapes and misplaced labels, the end-points of the breast border (denoted as C and D in Fig. 2) are determined by the maxima within the top and left margins of the image

$$x_C = \max\{x_{\text{border}} : 0 \leq y_{\text{border}} \leq 0.15n_y\} \quad (6)$$

$$y_D = \max\{y_{\text{border}} : 0 \leq x_{\text{border}} \leq 0.15n_x\}. \quad (7)$$

If for any reason the breast border is not available, x_C and y_D can be replaced by n_x and n_y , respectively. The validation criterion can then be described by the following expressions:

$$0 < x_A < x_C \quad \text{and} \quad 0 < y_B < y_D \quad (8)$$

where $(x_A, 0)$, $(0, y_B)$, $(x_C, 0)$, and $(0, y_D)$ are the coordinates of points A , B , C , and D , respectively. If the line is valid, *ROI adjustment* is invoked; otherwise *ROI shrinking* is performed. Details of these two methods are given in the following sections.

2) *ROI Adjustment*: The first ROI, R_1 , is only an initial estimate of the location of the pectoral edge. The ROI has to be *adjusted* so that the entire pectoral muscle is included, resulting in a more accurate straight line approximation. Therefore, a new ROI, \hat{R}_1 , is defined so that \overline{AB} runs diagonally from the top right corner to the left bottom corner in \hat{R}_1 , i.e.,

$$\hat{R}_1 = \{(x, y) : 0 \leq x < x_A \quad \text{and} \quad 0 \leq y < y_B\}. \quad (9)$$

Then, a *second* straight line estimation is performed on \hat{R}_1 , following the same procedure as described in Section IV-A. The result is used to update \overline{AB} . If the new straight line is also valid, it represents the best approximation to the pectoral edge from this stage of the algorithm; it is then ready to be refined into a curve by the iterative cliff detection, which is described in later sections.

3) *ROI Shrinking*: ROI shrinking is used when the straight line estimation is not valid. The result of invalid estimation could be due to internal texture or large artifacts on the pectoral muscle, but in most cases, the main cause is the breakdown of the assumption that the pectoral muscle occupies approximately half of the ROI. This smaller than expected pectoral muscle leads to an underestimated threshold. Shrinking the ROI so that the assumption is upheld is the basis for this step. If R_m is the current ROI, then the new ROI, R_{m+1} , is defined as the *top left quarter* of R_m , i.e.,

$$R_m = \left\{ (x, y) : 0 \leq x < \frac{n_x}{2^m} \quad \text{and} \quad 0 \leq y < \frac{n_y}{2^m} \right\}. \quad (10)$$

The same straight line estimation (described in Section IV-A) is performed on the new ROI in the hope that the result would be valid. The smallest possible ROI in this algorithm is R_4 , which is 1/256 of the original image size. If no valid straight line is found after R_4 is used, it is concluded that the pectoral edge cannot be detected, perhaps because it is absent altogether from the mammogram.

V. ITERATIVE CLIFF DETECTION

Cliff detection is designed to refine the straight line approximation into a curve that delineates the pectoral edge more accurately. The resulting curve is further refined by applying cliff detection multiple times; hence it is an iterative process. Finally, a roughly triangular region is enclosed to represent the segmented pectoral muscle.

A. Cliff Detection

Cliff detection is performed on the whole mammogram and not on any ROI. It consists of four steps:

1) *Defining Search Paths*: If the straight line estimation is accurate enough, the actual pectoral edge should be in close proximity to \overline{AB} . Therefore, *search paths* are used to find the exact position of the muscle edge in the vicinity of the straight line. The whole image is first smoothed by an average filter of size $m \times m$. On every pixel of \overline{AB} , a search path of length $2d$ is defined so that it is perpendicular to \overline{AB} and the distances on both sides of \overline{AB} are equal.

However, there is an exception at the image edges. Part of a search path could lie outside of the image if it is placed perpendicularly to \overline{AB} . In such cases, the search path is rotated in the appropriate direction so that its outlying end-point is moved back into the range of the image, just touching the image edge [see Fig. 7(a)].

An example of perpendicular and rotated search paths is shown as s_1 and s_2 , respectively, in Fig. 2. The rotated search paths may overlap each other, but this is acceptable. Although other orientations for the search paths were tried, the perpendicular orientation gave the best results, and was best suited to detect the intensity edge representing the pectoral margin.

Keeping the search path in full length is important because search path length and intensity surface smoothness are related. The smoother the intensity surface, the longer the search path that should be used to detect the intensity cliff. That is why search path length, d , and smoothing filter size, m , are *reduced together* in each iteration (see also Section V-B). Experiment has shown that shortening the search path at the image edge

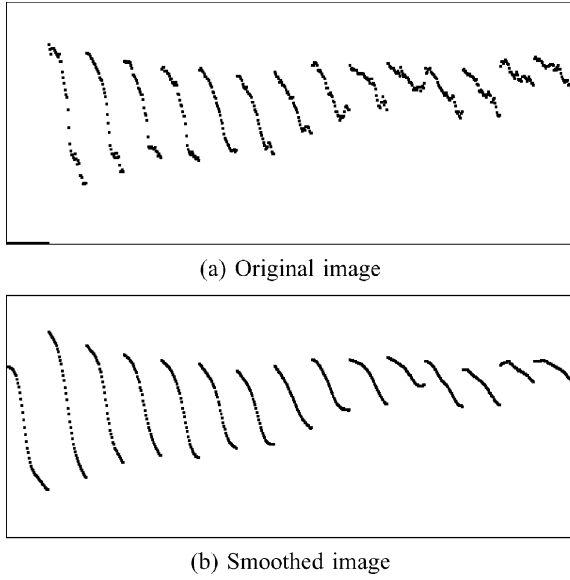


Fig. 5. Comparison of intensity profiles of original and smoothed images. Only every 20th profile is shown here.

results in less accurate cliff detection; while rotating the full length search path has a higher chance to include the cliff in the intensity profile.

2) *Extracting Intensity Profiles*: The next step is to extract *intensity profiles* along the search paths. The intensity profile, $P(k)$, is a function that represents the cross-section of the smoothed image surface on each search path. If there is a pectoral edge, a significant intensity drop, or a *cliff*, is expected on the intensity profile. Cliff detection is actually designed to locate the intensity cliff of the pectoral margin from a collection of intensity profiles across the straight line \overline{AB} . Fig. 5 illustrates the difference between intensity profiles of the original and smoothed images.

3) *Determining Cliff Locations*: The determination of the spatial coordinates of the intensity cliff is the next step in the algorithm. It was observed that most of the smoothed profiles exhibit a typical sigmoidal shape with various slopes and intensity changes. However, that typical shape did not necessarily appear in all profiles, as may be seen in the two rightmost profiles in Fig. 5(b). To confer robustness on the algorithm, it was decided to locate the cliff by fitting the smoothed profile to a *sigmoid function*.

This sigmoid function, $S(k; \alpha, \beta, p_{\max}, p_{\min})$, is a hyperbolic tangent function

$$S(k; \alpha, \beta, p_{\max}, p_{\min}) = \frac{p_{\max} - p_{\min}}{2} \tanh(\alpha - \beta k) + \frac{p_{\max} + p_{\min}}{2} \quad \text{for } k \in [0, 2d]; \beta > 0 \quad (11)$$

where p_{\max} and p_{\min} are the maximum and minimum intensities in $P(k)$, and α and β are fitting parameters solved by least squared error, i.e., $\varepsilon^2 = [S(k; \alpha, \beta, p_{\max}, p_{\min}) - P(k)]^2$ is minimized. Fig. 6 shows a plot of the sigmoid. The cliff location, k_c , is determined at the point of inflection of $S(k)$, i.e.,

$$k_c = \begin{cases} 0, & \text{if } \frac{\alpha}{\beta} < 0 \\ \frac{\alpha}{\beta}, & \text{if } 0 \leq \frac{\alpha}{\beta} \leq 2d \\ 2d, & \text{if } \frac{\alpha}{\beta} > 2d \end{cases} \quad (12)$$

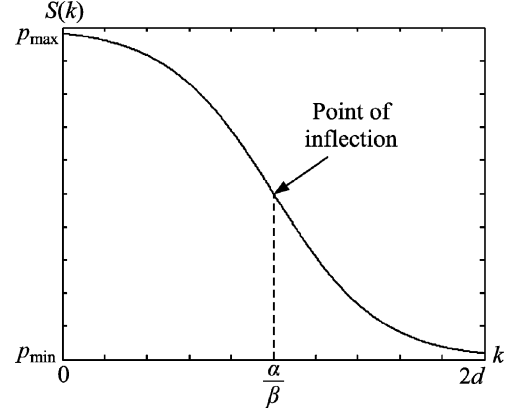


Fig. 6. The sigmoid model, $S(k)$, where α and β are fitting parameters; p_{\max} and p_{\min} are the maximum and minimum values of the smoothed profile, $P(k)$, respectively; $2d$ is the length of the corresponding search path. The point of inflection at $k_c = \alpha/\beta$ is assumed to be the cliff location on the intensity profile.

The cliff locations of all the extracted profiles are marked on a blank image, which has the same size as the original [see Fig. 7(b)]. This set of cliff locations is denoted by \mathcal{C} .

4) *Smoothing the Detected Curve*: The next step is to express the set of cliff locations as a function of y . This is done by eliminating certain cliff locations from \mathcal{C} , and adding intermediate values where necessary. If there is more than one cliff location for a given y value on a horizontal scan line, only that with the largest x value is retained; the others are eliminated. On the other hand, if there is no cliff location for a given y value on a horizontal scan line, two-point linear interpolation is used to generate an intermediate point. The resulting function is smoothed by a 24 mm wide moving-window average filter. Also, two strips of padding, 12 mm each, and parallel to line \overline{AB} , are added at both ends of the function to reduce distortion [see Fig. 7(c)]. This smoothed function is called the *detected curve* and is the output of cliff detection.

B. Iterative Refinement

Cliff detection can be applied iteratively to refine the detected curve. Since the image is smoothed before determining cliff locations, the sharpness of the pectoral edge is reduced, and hence the detected curve from the *first* cliff detection may be slightly inaccurate. Two previously defined variables of the algorithm, m and d , are set to 4 and 8 mm, respectively, in the first cycle of cliff detection. In the next iteration, m is decremented by 1 pixel and d by 2 pixels. Search paths are defined in the same way, but this time on the detected curve rather than the straight line. The same procedure is carried out as described in Section V-A to produce a new curve. The iterative process stops when either m or d is reduced to 1 pixel. During the curve refinement, the image surface is gradually *sharpened* together with a reduction in the maximum search distance. Consequently the final detected curve delineates the pectoral edge to a higher degree of accuracy. The final segmentation result for mammogram mdb227lm is depicted in Fig. 7(f).

C. Region Enclosing

Since the detected curve is a function of y , its top end always coincides with the top edge of the image. However, in some cases, its bottom end may not be aligned with the left edge of

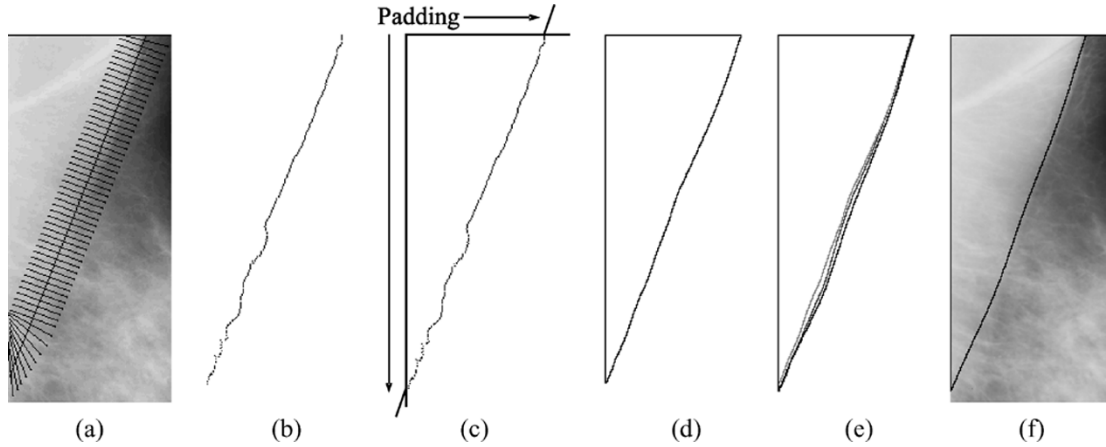


Fig. 7. Illustration of iterative cliff detection. (a) Search paths placed across the straight line \overline{AB} (only every fifth path is shown). (b) All the detected cliff locations. (c) Two pieces of padding, parallel to the straight line, are added at both ends of the detected curve for smoothing. (d) Detected curve after first iteration. (e) Detected curves after 1st, 5th and 9th iterations, respectively, from left to right. (f) Final segmentation of the pectoral muscle.

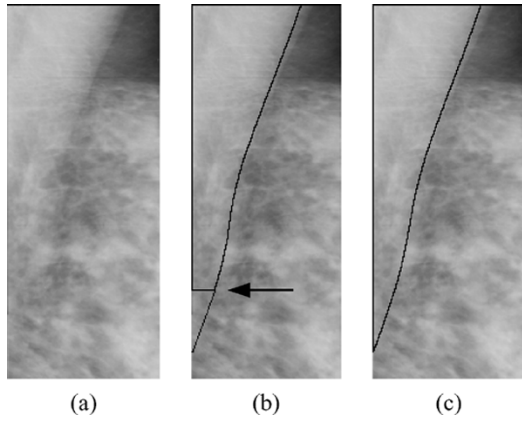


Fig. 8. (a) Pectoral muscle of MIAS image mdb2151l. (b) A straight line parallel to \overline{AB} is extended from the end of detected curve (marked by arrow). (c) Enclosed region for final segmentation.

the image. In order to form a closed region, the bottom end is extended by a straight line parallel to \overline{AB} (Fig. 2), after the final iteration, if necessary. The extended curve is then smoothed again by the 24 mm average filter. Finally, this enclosed region can be used to segment the pectoral muscle on the mammogram. It is pointed out that this extrapolation has been deliberately chosen to guarantee region closure using a line segment that is consistent with the overall direction of the pectoral margin. An example is illustrated in Fig. 8.

VI. EXPERIMENTAL SETUP

This new method for pectoral muscle segmentation was tested on 322 digitized mammograms from the MIAS database [22]. The original 50 $\mu\text{m}/\text{pixel}$ images were low-pass filtered and reduced in resolution to 400 $\mu\text{m}/\text{pixel}$. The original bit-depth of 8 bits [0–255] was retained.

Two expert mammographic radiologists were invited to assess the goodness of the segmentation; one of them is the last author of this paper. At the beginning of the assessment, they were acquainted with the purpose of segmentation, in order to better objectify the results and ensure consistency, thus:

The purpose of the segmentation is to localize the pectoral margin with sufficient accuracy so as to segment out the

“pectoral triangle” on mediolateral oblique mammograms. This will facilitate exclusion of muscular tissue with nonexclusion of parenchymal tissue, mammogram density analysis, parenchymal characterization, mammogram adequacy determination via nipple to pectoral margin perpendicular lines, etc.

The radiologists were then presented with the original mammograms and two types of segmented images: the straight line and curve segmentation of the pectoral muscles generated by straight line estimation and cliff detection, respectively. The segmented images were displayed on a computer screen in a random order. The segmentation boundary was colored in red and superimposed on the original mammogram, without any contrast enhancement. The radiologists were asked to assess all the images of straight line segmentation first. After that the images of curve segmentation were assessed in the same manner. For each image, the radiologists determined whether the segmentation was acceptable, which is a binary decision, and then, during a second pass, they rated the goodness of segmentation using a five-point scale, as explained in Table I. A score of 3 or less indicates an adequate segmentation.

VII. RESULTS

A. Radiologists' Assessments

The numbers of straight line and curve segmentation images accepted by the two radiologists are listed in Table II. It shows that radiologist 1 rated as acceptable 243 (75.5%) images for straight line segmentation and 280 (87.0%) images for curve segmentation; while radiologist 2 rated as acceptable 170 (52.8%) images for straight line segmentation and 216 (67.1%) images for curve segmentation. Although the segmentation images accepted by radiologist 2 are fewer than those accepted by radiologist 1, both radiologists agreed that after applying curve refinement the number of acceptable images increased.

The significance of the improvement can be determined statistically by the McNemar test [25, pp. 75–80]. This test is useful for detecting changes in initial and final responses (acceptable images) due to experimental intervention (curve segmentation). The test was performed using the contingency tables shown in

TABLE I
FIVE-POINT ASSESSMENT SCALE WITH SCORE DESCRIPTIONS

Score	Meaning	Description
1	Exact	The segmented straight line or curve delineates the pectoral margin exactly. Any deviations from the visually perceived margin are imperceptible or insignificant.
2	Optimal	The segmented straight line or curve delineates the pectoral margin exactly for at least half its length and adequately for the other half.
3	Adequate	The segmented straight line or curve delineates the pectoral margin inexactly but with sufficient accuracy for localizing the pectoral margin for the intended purpose.
4	Sub-optimal	The segmented straight line or curve delineates the pectoral margin inadequately for at least half its length.
5	Inadequate	The segmented straight line or curve is either absent or is so inaccurate as to be inadequate for localizing the pectoral margin for the intended purpose.

TABLE II
NUMBERS OF SEGMENTATION ACCEPTED BY THE TWO RADIOLOGISTS

Radiologist 1 Decision	Straight Line Segmentation		Curve Segmentation	
	Number	Percentage	Number	Percentage
Acceptable	243	75.5%	280	87.0%
Not Acceptable	79	24.5%	42	13.0%

Radiologist 2 Decision	Straight Line Segmentation		Curve Segmentation	
	Number	Percentage	Number	Percentage
Acceptable	170	52.8%	216	67.1%
Not Acceptable	152	47.2%	106	32.9%

Table III. The McNemar chi-squared test statistics and approximated P-values are 33.23 and 8.18×10^{-9} for radiologist 1, and 24.11 and 9.11×10^{-7} for radiologist 2. Since the P-values are very small in both cases, we conclude that *curve segmentation has improved the accuracy of pectoral muscle segmentation*. The contingency tables also show that after curve segmentation, 38 images were upgraded from not acceptable to acceptable for radiologist 1, and 65 images for radiologist 2. On the other hand, only 1 image was downgraded from acceptable to not acceptable for radiologist 1, and 19 images for radiologist 2.

The radiologists' five-point ratings for the 322 straight line segmentation images and 322 curve segmentation images are shown in Table IV. The results show that radiologist 1 rated the straight line segmentation *adequate or better* on 243 (75.5%) images and the curve segmentation *adequate or better* on 286 (88.8%) images. The same figures for radiologist 2 are 197 (61.2%) and 258 (80.1%), respectively. Again, the ratings of radiologist 2 are lower than that of radiologist 1, but in both cases the ratings were improved (by 13.3% and 18.9%) after applying curve segmentation. By taking the average score of each image, 67.4% of the straight line segmentation and 83.9% of the curve segmentation were rated adequate or better (≤ 3).

Furthermore, after curve refinement, the ratings given by radiologist 1 increased on 164 (50.9%) images, remained unchanged on 141 (43.8%) images and decreased on 17 (5.3%) images. The same figures for radiologist 2 are 147 (45.7%),

TABLE III
CONTINGENCY TABLES OF STRAIGHT LINE AND CURVE SEGMENTATION

Radiologist 1	Curve	
Straight Line	Acceptable	Not Acceptable
Acceptable	242	1
Not Acceptable	38	41

Radiologist 2	Curve	
Straight Line	Acceptable	Not Acceptable
Acceptable	151	19
Not Acceptable	65	87

TABLE IV
SEGMENTATION ACCURACY RATINGS BY THE TWO RADIOLOGISTS

Radiologist 1 Rating (Score)	Straight Line Segmentation		Curve Segmentation	
	Number	Percentage	Number	Percentage
Exact (1)	84	26.1%	169	52.5%
Optimal (2)	106	32.9%	85	26.4%
Adequate (3)	53	16.5%	32	9.9%
Sub-optimal (4)	33	10.2%	10	3.1%
Inadequate (5)	46	14.3%	26	8.1%

Radiologist 2 Rating (Score)	Straight Line Segmentation		Curve Segmentation	
	Number	Percentage	Number	Percentage
Exact (1)	34	10.6%	87	27.0%
Optimal (2)	50	15.5%	54	16.8%
Adequate (3)	113	35.1%	117	36.3%
Sub-optimal (4)	59	18.3%	30	9.3%
Inadequate (5)	66	20.5%	34	10.6%

152 (47.2%), and 23 (7.1%), respectively. Therefore, by refining the straight lines into curves, almost half of the image ratings increased by one level or more. These results once again demonstrated that pectoral muscle segmentation was more accurate after applying iterative cliff detection.

As mentioned previously in Section VI, the radiologists assessed the images in two passes using two different scales. Therefore, "acceptable" in Table II is *not necessarily* equivalent to "adequate or better" in Table IV. The difference between the two sets of results illustrates the uncertainty encountered in human observer studies, especially when two different rating scales are given.

The 5×5 contingency tables of the segmentation ratings are shown in Table V to give the readers an insight into the *correlation* or *agreement* between both radiologists. Since our 5-point scale is an ordinal measurement, the Spearman rank-order correlation coefficient [25, pp. 235–244], r_s , was used to evaluate the association between the radiologists' ratings. For the straight line segmentation ratings, r_s is 0.740 and the P-value is 4.54×10^{-57} . For the curve segmentation ratings, r_s is 0.748 and the P-value is 6.27×10^{-59} . Since the P-values are very small in both cases, we conclude that the positive correlation between the ratings given by both radiologists is statistically significant at the 1% level.

B. Algorithm Performance

The average processing time for a single mammogram was around 5.9 s, in which 0.4 s was spent on straight line estimation

TABLE V
CONTINGENCY TABLES OF RADIOLOGISTS' RATINGS

Straight Line	Radiologist 2				
Radiologist 1	Exact	Optimal	Adequate	Sub-optimal	Inadequate
Exact	30	27	25	1	1
Optimal	2	21	53	29	1
Adequate	1	1	25	19	7
Sub-optimal	0	0	9	7	17
Inadequate	1	1	1	3	40

Curve	Radiologist 2				
Radiologist 1	Exact	Optimal	Adequate	Sub-optimal	Inadequate
Exact	85	34	50	0	0
Optimal	2	18	53	12	0
Adequate	0	2	14	13	3
Sub-optimal	0	0	0	5	5
Inadequate	0	0	0	0	26

and 5.5 s on iterative cliff detection. The computational time for curve refinement is much longer than that for straight line estimation because the former is an iterative process, in which the whole image has to be smoothed multiple times with filters of different sizes.

In straight line estimation, ROI shrinking was performed on 40 images, i.e., the straight line did not pass the first validation in those cases. In the end, a valid straight line could be found on 34 of those images: so shrinking the ROI is a necessary step when the pectoral muscle is smaller than normal. The straight line estimation was not successful on the other 6 images, hence there was no curve segmentation for these images as well. In addition, the curve extension used to enclose the pectoral region was performed on 195 images. The average length of the extended line was approximately 5.5 mm, which is relatively small on the mammogram.

Some examples of the final segmentation are shown in Fig. 9. The full set of segmentation results are available online at <http://users.arcme.com/skwok/>.

VIII. DISCUSSION

The algorithm is adaptive to variations in pectoral muscle size, density and curvature. In an adequate mammogram, the pectoral muscle should be visible down to the level of the nipple [4]. In some extreme cases, however, the muscle may appear on the mammogram as very small or very large. Two examples of tiny and large pectoral muscles are shown in Fig. 9(a) and (b). They were both segmented accurately because multiple ROIs, from large to small, were used in the straight line estimation. Also, there is a variation on the image intensities of different pectoral muscles. We found that the method of iterative threshold selection can adaptively compute an appropriate threshold level for each image, provided that the pectoral region occupies roughly 50% of the ROI. Furthermore the segmentation method was accurate for tracing pectoral boundaries of different curvatures, whether convex, concave or both.

Sometimes there may be more than one layer of tissue in the pectoral region and more than one edge may be depicted.

In such cases the straight line approximation is more likely to be placed at the outer edge rather than at the inner edge. The reasons for this are that 1) the straight line estimation method uses histogram thresholding instead of edge detection to find the edge; and 2) the straight line is fitted only to that segment of the selected pixels which encloses the largest area. Therefore, the outer edge is more likely to be chosen. Fig. 9(c)–(e) shows pectoral muscles with internal edges of different edge strengths and they are all delineated at the outer edges.

The results also demonstrate that the segmentation method is robust against artifacts such as sticky tapes. Fig. 9(f) and (g) show that although the top parts of the pectoral muscles are obscured by tapes of different thickness, both were segmented successfully. These images show one of the advantages of cliff detection: the refinement of the straight line is restricted in certain directions, since the search paths are set perpendicularly, and only intensity *decreases* in the profiles are searched for. Also, the detected curve in each iteration is smoothed so that no sharp corners on the curve are allowed. More examples of different kinds of small edges crossing the pectoral boundary are shown in Fig. 9(h)–(j).

In Fig. 9(k), a very dense breast is shown and the lower half of the pectoral muscle is almost completely obscured by other tissues. In this case, the extrapolative power of the segmentation method is demonstrated. The pectoral boundary was extended following the direction of the estimated straight line. And the refinement process did not alter the extended line significantly since there were no other strong intensity changes within the reach of the search paths.

One disadvantage of the proposed, intensity-based method is its weakness in detecting texture edges. In some cases the pectoral boundary is not a clear intensity edge but a fuzzy texture edge. Cliff detection is not a suitable method to detect edges between different textures. However it can still be used to approximate the pectoral boundary based on the intensity changes alone. An example is illustrated in Fig. 9(l).

Another shortcoming relates to the detection of vertical pectoral edges, which are excluded by assumption. Because a valid straight line approximation is assumed to intersect the top and left image edges, a vertical line cannot satisfy the validation criterion. As shown in Fig. 9(m) the pectoral edge is almost vertical but it was not segmented correctly.

A very poor segmentation is shown in Fig. 9(n), which is a particularly difficult image due to the coarse texture in the muscle region. Finally, no segmentation was produced for Fig. 9(o). The pectoral edge of this image is barely visible. The primary reason for no segmentation is that the pectoral muscle does not exist on the image, or that a large part of the pectoral margin is obscured by dense tissue.

The radiologists also made the following comments for poorly segmented images. For some images, the straight lines were placed *parallel* to the pectoral margins but not exactly on them. Poor straight line estimation also resulted when the pectoral margins were very curved. These kinds of inaccuracy, especially in the straight line estimation, were normally corrected by the iterative refinement in curve segmentation [see Fig. 10(a) and (b)]. However, in a small number of cases, some straight lines completely missed the pectoral margins due to the influence of the *axillary fold*, which appears as a high-intensity

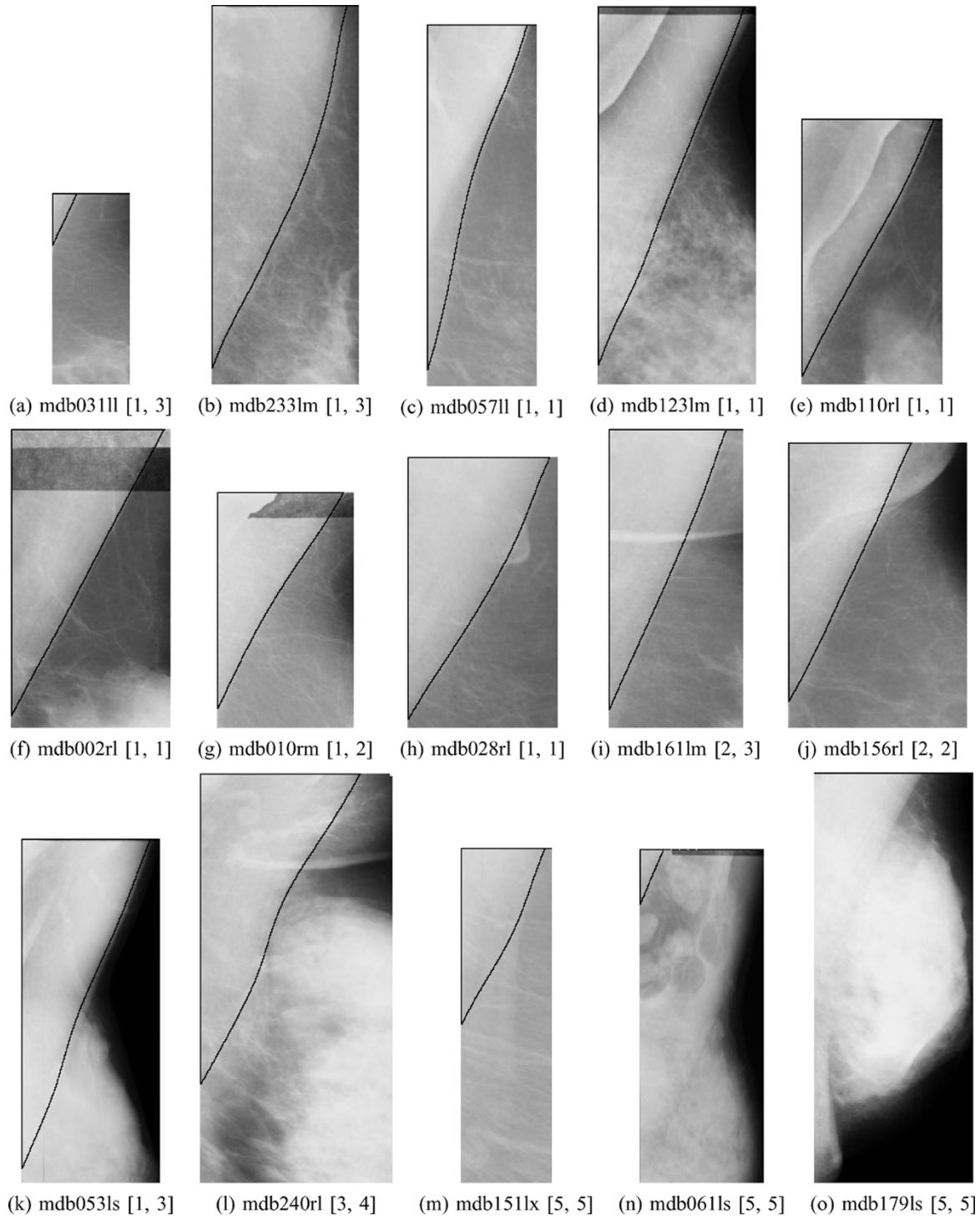


Fig. 9. Segmentation results on MLO mammograms from the MIAS database. The scores of each image rated by two radiologists are shown in $[r_1, r_2]$. All images are shown in the same scale. There was no segmentation for (o).

triangular region, similar to the pectoral muscle [see Fig. 10(c)]. The radiologists also noted that the axillary fold should not normally be seen on the MLO view and that its presence is often the result of poor positioning.

The proposed algorithm could be improved in future by incorporating a texture edge detector together with cliff detection. This is particularly targeted at extracting the texture edge at the lower portion of the pectoral muscle. Such a texture edge de-

tector should be sensitive to texture direction since the texture direction of the pectoral margin is usually perpendicular to that of the overlying glandular tissue. Also texture detection should be carried out at higher image resolutions than the one used in cliff detection.

Most of the other difficulties in segmentation result from a poor positioning of the patient during image acquisition or to poor image contrast. Thus, one way to overcome these problems

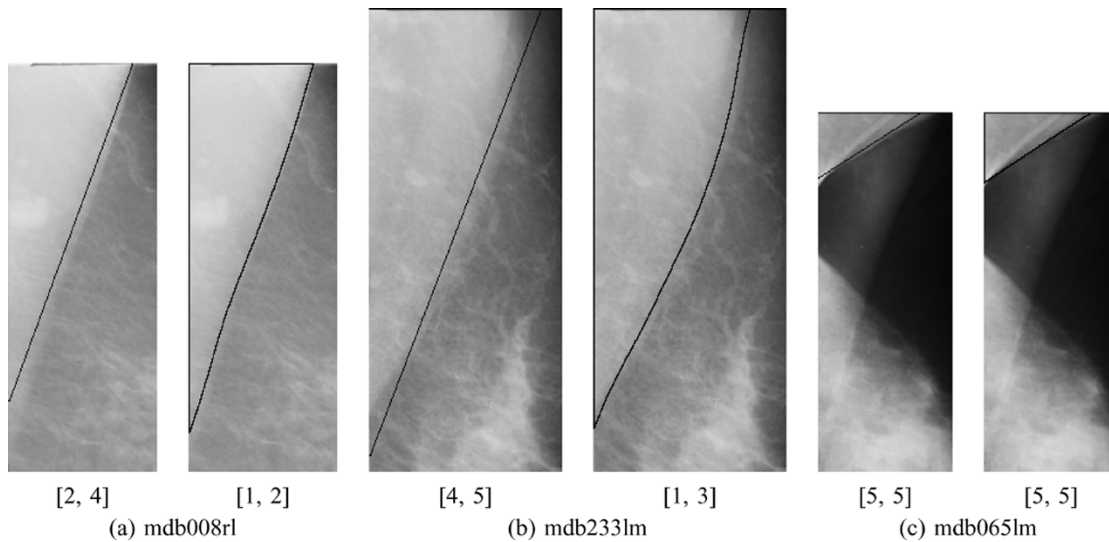


Fig. 10. Comparison of straight line and curve segmentation results on mammograms from the MIAS database. The scores of each image rated by two radiologists are shown in $[r_1, r_2]$. (a) The straight line (left) is roughly parallel to the pectoral margin but not exactly on it. This is corrected in curve segmentation (right). (b) The pectoral muscle is poorly segmented by the straight line (left) but accurately segmented by the curve (right). (c) The axillary fold is mistakenly segmented by the straight line (left) and hence the curve (right) is also inadequate. Moreover, hypothesis (2) is not valid for this image.

would be to ensure acquisition of good quality images in the first place. We have suggested elsewhere [15] that automatic quality assurance during image acquisition is a feasible solution to this problem. When the breast is correctly positioned, a sufficient amount of pectoral muscle should be seen to the level of the nipple at an angle larger than 20° to the vertical edge [14]. When the image is properly exposed at optimal contrast, the pectoral muscle should be differentiated from other dense tissue more easily.

IX. CONCLUSION

We have developed a new method for automatic segmentation of the pectoral muscle on the MLO views of mammograms. The method consists of two major components: straight line estimation and iterative cliff detection. By approximating the pectoral boundary with a straight line and refining it iteratively to a curve, it is possible to accurately delineate an enclosed pectoral region. The method was adaptive to large variations in appearance of the pectoral muscle and margin. The method remained effective when parts of the pectoral edge were obscured by superimposed glandular tissue or artifacts. The method was tested out on the 322 digitized mammograms of the MIAS database and two mammographic radiologists assessed the segmentation results. Their findings show that segmentation accuracy was improved after refining the straight line into a curve using iterative cliff detection and that 83.9% of the curve segmentations were adequate or better.

ACKNOWLEDGMENT

The authors would like to thank Dr. N. Borecky, of BreastScreen NSW, who also assessed the segmentation results. The authors would also like to thank Prof. I. James, of Murdoch University, and Dr. D. Milech, of The University of Western Australia, for their helpful advice on analyzing the results and providing expert guidance in statistics.

REFERENCES

- [1] R. Chandrasekhar and Y. Attikiouzel, "Automatic breast border segmentation by background modeling and subtraction," in *IWDM 2000: 5th Int. Workshop Digital Mammography*, M. J. Yaffe, Ed., Toronto, ON, Canada, June 11–14, 2000, pp. 560–565.
- [2] —, "A simple method for automatically locating the nipple on mammograms," *IEEE Trans. Med. Imag.*, vol. 16, pp. 483–494, Oct. 1997.
- [3] S. M. Kwok, R. Chandrasekhar, and Y. Attikiouzel, "Automatic pectoral muscle segmentation on mammograms by straight line estimation and cliff detection," in *Proc. 7th Australian and New Zealand Intelligent Information Systems Conf.*, Perth, Western Australia, Nov. 2001, pp. 67–72.
- [4] G. W. Eklund, G. Cardenosa, and W. Parsons, "Assessing adequacy of mammographic image quality," *Radiology*, vol. 190, no. 2, pp. 297–307, Feb. 1994.
- [5] R. Gupta and P. E. Undrill, "The use of texture analysis to delineate suspicious masses in mammography," *Phys. Med. Biol.*, vol. 40, pp. 835–855, 1995.
- [6] Y. Hatanaka, T. Hara, H. Fujita, S. Kasai, T. Endo, and T. Iwase, "Development of an automated method for detecting mammographic masses with a partial loss of region," *IEEE Trans. Med. Imag.*, vol. 25, pp. 5209–1212, Dec. 2001.
- [7] N. Karssemeijer, "Automated classification of parenchymal patterns in mammograms," *Phys. Med. Biol.*, vol. 43, no. 2, pp. 365–378, Feb. 1998.
- [8] P. K. Saha, J. K. Udupa, E. F. Conant, D. P. Chakraborty, and D. Sullivan, "Breast tissue density quantification via digitized mammograms," *IEEE Trans. Med. Imag.*, vol. 20, pp. 792–803, Aug. 2001.
- [9] M. Yam, M. Brady, R. Highnam, C. Behrenbruch, R. English, and Y. Kita, "Three-dimensional reconstruction of microcalcification clusters from two mammographic views," *IEEE Trans. Med. Imag.*, vol. 20, pp. 479–489, June 2001.
- [10] F. Georgsson, "Algorithms and techniques for computer aided mammographic screening," Ph.D. dissertation, Umeå Univ., Dept. Comput. Sci., Umeå, Sweden, 2001.
- [11] P. Miller and S. Astley, *Automated Detection of Breast Asymmetry using Anatomical Features*. ser. Machine Perception and Artificial Intelligence, K. W. Bowyer and S. Astley, Eds, Singapore: World Scientific, 1994, vol. 9, pp. 247–261.
- [12] G. W. Eklund and G. Cardenosa, "The art of mammographic positioning," *Radiologic Clin. N. Amer.*, vol. 30, no. 1, pp. 21–53, Jan. 1992.
- [13] L. W. Bassett, I. A. Hirbawi, N. DeBruhl, and M. K. Hayes, "Mammographic positioning: Evaluation from the view box," *Radiology*, vol. 188, pp. 803–806, 1993.
- [14] S. H. Heywang-Köbrunner, D. D. Dershaw, and I. Schreer, *Diagnostic Breast Imaging: Mammography, Sonography, Magnetic Resonance Imaging, and Interventional Procedures*, 2nd ed. Stuttgart, Germany: Georg Thieme Verlag, 2001.

- [15] R. Chandrasekhar, S. M. Kwok, and Y. Attikiouzel, "Automatic evaluation of mammographic adequacy and quality on the mediolateral oblique view," in *Digital Mammography: IWDM 2002: Proc. 6th Int. Workshop Digital Mammography*, H.-O. Peitgen, Ed., Bremen, Germany, June 22–25, 2002, pp. 182–186.
- [16] R. J. Ferrari, R. M. Rangayyan, J. E. L. Desautels, and A. F. Frère, "Segmentation of mammograms: Identification of the skin boundary, pectoral muscle, and fibroglandular disc," in *IWDM 2000: Proc. 5th Int. Workshop Digital Mammography*, M. J. Yaffe, Ed., Madison, WI, 2001, pp. 573–579.
- [17] J. Suckling, D. R. Dance, E. Moskvic, D. J. Lewis, and S. G. Blacker, "Segmentation of mammograms using multiple linked self-organizing neural networks," *Med. Phys.*, vol. 22, no. 2, pp. 145–152, Feb. 1995.
- [18] S. R. Aylward, B. M. Hemminger, and E. D. Pisano, "Mixture modeling for digital mammogram display and analysis," in *Digital Mammography: Nijmegen, 1998*, N. Karssemeijer, M. Thijssen, J. Hendriks, and L. van Erning, Eds. Dordrecht, The Netherlands: Kluwer Academic Publishers, 1998, vol. 13, Computational Imaging and Vision, pp. 305–312.
- [19] P. K. Sinha, J. K. Udupa, E. F. Conant, and D. P. Chakraborty, "Near automatic quantification of breast tissue glandularity via digitized mammograms," in *Proc. SPIE: Medical Imaging 1993*, K. M. Hanson, Ed. San Diego, CA, USA: SPIE, 1999, vol. 3661, SPIE Proceedings, pp. 266–276.
- [20] R. Chandrasekhar and Y. Attikiouzel, "New range-based neighborhood operator for extracting edge and texture information from mammograms for subsequent image segmentation and analysis," *IEE Proceedings—Science, Measurement and Technology*, vol. 147, no. 6, pp. 408–413, Nov. 2000.
- [21] —, "Segmentation of the pectoral muscle edge on mammograms by tunable parametric edge detection," in *Advances in Signal Processing and Computer Technologies*, G. Antoniou, N. Mastorakis, and O. Panfilov, Eds. Athens, Greece: World Scientific and Engineering Society WSES Press, 2001, pp. 55–60.
- [22] J. Suckling, J. Parker, D. R. Dance, S. Astley, I. Hutt, C. R. M. Boggis, I. Ricketts, E. Stamatakis, N. Cerneaz, S.-L. Kok, P. Taylor, D. Betal, and J. Savage, "The mammographic image analysis society digital mammogram database," in *Digital Mammography*, A. G. Gale, S. M. Astley, D. R. Dance, and A. Y. Cairns, Eds. Amsterdam, The Netherlands: Elsevier Science, 1994, vol. 1069, Excerpta Medica International Congress Series, pp. 375–378.
- [23] A. Magid, S. R. Rotman, and A. M. Weiss, "Comment on 'Picture thresholding using an iterative selection method'," *IEEE Trans. Syst., Man, Cybern.*, vol. 20, pp. 1238–1239, Sept./Oct. 1990.
- [24] M. Sonka, V. Hlavac, and R. Boyle, *Image Processing, Analysis, and Machine Vision*, 2nd ed. Pacific Grove, CA: PWS Publishing, 1999.
- [25] S. Siegel and N. J. Castellan Jr., *Nonparametric Statistics for the Behavioral Sciences*, 2nd ed. New York: McGraw-Hill, 1988.